Journal of Translational Science

Research Article ISSN: 2059-268X

3D finite element model of posterior membranous labyrinth from in vivo MRI of human temporal bone, including sensory zones

Chaney HV[1]*, Lamy M[2], Baumgartner D[3], Venkatasamy A[4], Veillon F[5], Rohmer D[6], Riehm S[7], Debry C[8] and Charpiot A[9]

[1]Assistant, ORL, CHU Hautepierre, Avenue Molière, 67098 Strasbourg cedex, France

[2]Engineer, Strasbourg University, France

[3]MCU, Strasbourg University, France

[4]CCA, Radiology, CHU Hautepierre, Avenue Molière, 67098 Strasbourg cedex, France

[5]PU-PH, Radiology, CHU Hautepierre, Avenue Molière, 67098 Strasbourg cedex, France

[6]PH, ORL, CHU Hautepierre, Avenue Molière, 67098 Strasbourg cedex, France

[7]PH, Radiology, CHU Hautepierre, Avenue Molière, 67098 Strasbourg cedex, France

[8]PU-PH, ORL, CHU Hautepierre, Avenue Molière, 67098 Strasbourg cedex, France

[9]PU-PH, ORL, CHU Hautepierre, Avenue Molière, 67098 Strasbourg cedex, France

Abstract

Objective: The aim of this work is to create a three-dimensional (3D) finite element model (FEM) of the human posterior membranous labyrinth, based on *in vivo* inner ear magnetic resonance imaging (MRI).

Study design and setting: We used T2 weighted gradient-echo 3T MRI of a human inner ear. Images were acquired *in vivo*, from a patient presenting a vestibular schwannoma with a preserved labyrinthine geometry. Indeed, in this context, the elevation of the perilymphatic protides level secondary to the obstructive vestibular schwannoma enables a differentiation between the endolymph (which remains hyperintense on T2 weighted images) and the perilymph (hypointense on T2 weighted gradient echo images).

Results: A 3D reconstruction of the posterior membranous labyrinth was performed through manual segmentation of the endolymphatic and sensory spaces. A mesh of the labyrinth was realized, first of its outer surface and then of its interior volume. The different structures of the labyrinth are included through a compartmentalization of the mesh. Sensory zones are precisely defined, based on a radio-histological correlation study. The resulting mesh of the model included 124,701 elements.

Conclusion: Dimensions are in agreement with those in the literature, which is in favor of the validity of the model geometry. This model also has a pedagogical interest and can be useful for the clinical reflexion in cases of atypical benign paroxysmal positional vertigos (BPPV). It can also serve as a base for mechanical studies of vestibular physiology.

Key points

1. This 3D model is based on *in vivo* inner ear imaging.
2. It is a FEM of human posterior membranous labyrinth.
3. This model includes all the sensory zones of the posterior membranous labyrinth.

Abbreviations: 3D: three-dimensional; BPPV: benign paroxysmal positional vertigos; CT: computed tomography; FEM: finite element model; FIESTA: Fast Imaging Employing Steady State Acquisition; MRI: magnetic resonance imaging; SCC: semi-circular canal; STL: stereolithography.

Introduction

A morphologically precise 3D model of the posterior membranous labyrinth of the inner ear is a powerful tool for a better understanding of the vestibular physiology. It also offers an educational interest for mental representation of the orientation of human semi-circular canals (SCC) and their sensory zones. It could also prove useful in the learning process of vestibular positional manoeuvers. Likewise, it presents a clinical interest, as it can serve as a basis for diagnosis reasoning in cases of atypical BPPV.

Correspondence to: Hella VUONG CHANEY, Otorhinolaryngology Service and cervico-facial surgery, CHRU Hautepierre, Avenue Molière, 67098 Strasbourg Cedex, France, E-mail: hella.vuong@chru-strasbourg.fr

Key words: *inner ear, in vivo, finite element modeling*

Received: December 17, 2018; **Accepted:** January 19, 2019; **Published:** January 21, 2019

Other 3D models of the complete posterior human labyrinth have been created, but most of them have been constructed from *post mortem* human temporal bones or issued from animal models. Only a few 3D models of the human membranous posterior labyrinth have been created. Teranishi and al [1] developed a 3D model of the endolymphatic and perilymphatic spaces of the inner ear, using sections of human temporal bones with and without hydrops. Rajguru and al [2] made a model of the human posterior membranous labyrinth, by reconstructing human sections of temporal bones. David and al developed 3D models of the human posterior membranous labyrinth by using X-ray micro computed tomography (CT) and tissue staining with phosphotungstic acid and created a software toolbox for morphological and functional analysis of the duct system [3].

To our knowledge, our model is the first 3D FEM of the human posterior membranous labyrinth that was reconstructed using *in vivo* MRI images, by segmentation of the endolymph and sensory zones. Moreover, that model specifies the position of all the sensory zones.

Reconstruction of the posterior membranous labyrinth was realized by a segmention of human temporal bone images. They were acquired *in vivo*, using a T2 weighted gradient-echo MR images acquired at 3T, from a patient presenting an obstructive vestibular schwannoma with a preserved labyrinth geometry and without labyrinthine extension of the tumor. In the presence of a vestibular schwannoma of the internal auditory canal, the geometry of the membranous labyrinth can be considered normal in approximately 70% of the cases, but the elevation of the perilymphatic protides concentration, resulting in a drop of the perilymphatic signal on T2 weighted gradient echo images enables to differentiate the endolymph, which signal remains normal, and the hypointense perilymph.

After a 3D segmentation of the posterior labyrinth, the resulting surface object (a net of points on said surface) was used to create the mesh of a 3D FEM. FEM are powerful tools for the estimation of a numerical solution to complex problems, in particular in structural mechanics. In the FEM, the modeled system exists as a discrete representation of its whole volume. The points of discretization are called the nodes: when interconnected, they are the vertices of cells. Those cells are the so-called finite elements. Elements can be attributed mechanical properties, to describe the materials they represent, and can be submitted to exterior or interior inputs. This technique thus offers new insights to complex biomechanical problems, which would be impossible to observe, measure or analyze *in vivo*.

Materials and methods

Preliminary histological and radiological studies of the sensory zones

We used the anatomical and histological atlas from Sick and Veillon, composed of 140 horizontal slices, 250 frontal slices and 300 sagittal slices of temporal bones, as reference for positioning of the sensory zones [4]. The material from this atlas comes from eight premature babies, born after 7 months of gestation. At this age, the development of the inner ears cavities has reached a state where they are similar to adult ones [5]. Sections were 10 to 12 µm thick and have been realized in the plane of the SCC, allowing a good correlation between radiological and histological studies. We also compared our observations with the histological works of Curthoys et al [6] and of Schuknecht et al. [7,8].

3D reconstruction of the posterior membranous labyrinth

In vivo images of the right inner ear were acquired from a patient with vestibular schwannoma (grade II), with a preserved membranous labyrinth geometry and no intralabyrinthite extension of the tumor (Table 1). In the presence of schwannoma, the elevation of the protides concentration in the perilymph space, resulting in a drop of the perilymphatic signal on gradient echo MR images, increases the contrast between the endolymphatic and perilymphatic spaces, as the endolymph remains normal [9]. This makes possible the tracing of the contours of the endolymphatic space. The membranous labyrinth geometry is conserved in about 70% of the cases, as we observed in our service about 30% of endolymphatic hydrops associated with schwannoma.

The patient underwent an axial high-resolution T2W three-dimensional (3D) gradient-echo FIESTA-C sequence at 3T (Signa HDxt, General Electric, *BLINDED*), using an eight-channel head coil. This sequence is a sort of modified steady state free precession sequence, which does not require any contrast injection. The study box was placed parallel to the orbital roof, extended from the orbital roof, downwards on 2.3 cm. The acquisition parameters were as follows: echo time (TE) = 0.8–1.2ms, repetition time (TR) = 7ms, field of view (FOV) = 22× 19.80 cm, frequency × phase = 484 × 484, flip angle = 60°C, number of excitations (NEX) = 1, bandwidth = 83.3 kHz, partition thickness = 0.3 × 0.3 × 0.3 mm (isotropic voxel). The acquisition time was 7 min 49 s.

The reconstruction of the inner ear was performed through a manual segmentation, on the images of the endolymphatic space and of the sensory zones, using the software ITK-Snap [10,11]. As the endolymph appears in a normal hyperintense signal on T2 weighted images, and the sensory zones appears hypointense, it was not possible to reconstruct the whole posterior membranous labyrinth volume with an automatic segmentation process. Therefore, we performed a manual voxel by voxel segmentation (as featured in Figure 1). Written informed consent was obtained from the patient for this study, and the Ethic committee approved the study (approval number FC/dossier 2017-31).

Figure 1. Axial slice of the right horizontal SCC and utricle. The membranous labyrinth is manually segmented, in order to include the endolymph (hypersignal) and the sensory zones (hyposignal).

In the canals themselves, the contrast between endolymph and perilymph was less obvious. The segmentation had to rely on histological knowledge: the membranous duct occupies about one quarter of the bone canal and is fixed on its external diameter [12]. This knowledge was used to confirm which voxels were to be part of the segmentation in the SCC.

Table 1. Dimensions of the model against data from the literature

	Measured axis	Dimension of the model (mm)	Literature data (mm)
A	Transversal axis of the saccule	1.06	1 to 1.4 (mean 1.2 mm) *(12)*
B	Cranio-caudal axis of the saccule	1.43	1 to 1.6 (mean 1.3 mm) *(12)*
C	Lateral cupula: width	0.3	0.3 *(12)*
D	Anterior cupula: width	0.3	0.3 *(12)*
E	Posterior cupula: width	0.3	0.3 *(12)*
F	Utricle: height	1.33	1.4 *(12)*
G	Utricle: major axis's length	4.71	5 *((12)*
H	Utricle: width	2.61	2.69 +/- 0.25 *(6)*
I	Lateral ampulla: diameter	2.02	2.1 (10) 1.75 +/- 0.16*(6)*

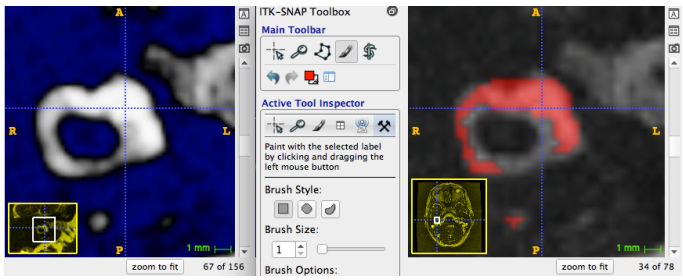

Figure 1. Axial slice of the right horizontal SCC and utricle. The membranous labyrinth is manually segmented, in order to include the endolymph (hypersignal) and sensory zones (hyposignal)

Once the whole volume of the membranous labyrinth was segmented, ITK-Snap software was used to obtain a first representation of its external surface, as a stereolithography (STL) file. This STL file contained a triangular surface mesh and was then imported in the Hypermesh software from the Altair Hyperworks software suite. We identified the different structures of the inner ear in the surface mesh, to classify the triangles in different components. The resulting compartmentalization included: the ampullas, the arms of the semi-circular canals, the crista and cupula of each ampulla, the short arm of the posterior canal, the common crus, the utricle, the utricular macula, the saccule, and the saccular macula. We also identified the parts of the model corresponding to the membranes which are attached to the bony canal. Therefore, we subdivided some components into "fixed" parts and "mobile" parts where needed. This whole identification process was based on histological knowledge [4].

However, the imaging modalities had generated some imperfections in this initial mesh. Indeed, the diameter of the membranous labyrinth, in the arms of the canals was about 0.3 to 0.4 mm, which was close to the voxel size. Consequently, the manual segmentation had to exclude some voxels that only partially contained endolymph data. This caused some local depressions in the meshes of the arms. We manually corrected these volume losses in the semi-circular canals, by deleting faulty elements and creating new ones where the surface should be (in accordance with observations and dimensions from the histological study). To further improve this reconstruction, the model was then smoothed with Meshlab software [11]. We used a Laplacian Smooth filter, as it allowed to streamline the canals without changing their diameters.

Results

Histological and radiological studies of the sensory zones

Horizontal SCC: The histological study shows the invariance of the position of the horizontal duct crista: it is inserted at the anterior part of the ampulla, perpendicular to its major axis (Figure 2a). There is a strong correlation with MRI findings: the crista appears in hypointense on T2 weighted images and is localized at the anterior part of the ampulla (Figure 2b). The ampulla of the lateral SCC is connected to the anterior part of the lateral wall of the utricle. The other extremity of the lateral SCC is attached to the posterior part of the lateral wall of the utricle. Meanwhile, the membranous duct is attached to the external quarter of the bony conduct [4]. The SCC displays an elliptic shape in its duct area, whereas next to the ampulla, the changes in the radiuses produce a more circular section shape [4].

Figure 2a: Histological slice of a human inner ear showing the anterior insertion of the crista in the horizontal duct ampulla [4]. **Figure 2b:** Axial slice of the right semicircular duct in a vestibular schwannoma (3T MRI). The contrast between the endolymphathic and perilymphatic spaces is increased. The lateral crista appears in hyposignal (1: perilymph, 2: lateral crista, 3: lateral ampulla filled with endolymph, 4: utricle). **Figure 2c**: Axial section of the horizontal SCC duct of a normal inner ear (3T MRI FIESTA sequence). 5: The lateral crista appears in hyposignal [12].

Anterior SCC

The crista of the anterior SCC is inserted at the antero-external and inferior part of the anterior ampulla (Figure 3). The anterior ampulla is connected to the upper part of the utricle. The other extremity of the anterior canal is attached to the common crus.

Figure 3a: Frontal histological slice of the human inner ear. The crista of the anterior semicircular duct is visible at the antero-external part of the ampulla [4]. 1: anterior duct, 2: lateral crista, 3: lateral duct, 4: horizontal part of the utricular macula, 5: saccular macula. **Figure 3b**: Sagittal slice of the anterior semicircular ampulla (3T Siemens MRI, Fiesta sequence [12]). 1: anterior duct, 2: anterior ampulla, 3: anterior crista appearing in hyposignal, 4: posterior duct, 5: common crus, 6: posterior duct.

Posterior SCC: The crista of the posterior SCC is localized at the anterior part of the ampulla of the posterior SCC. This SCC has a distinctive feature compared to the anterior and lateral SCC: its ampulla is joined to the utricle by a thin duct, known as the short arm of the posterior canal. The other extremity of the posterior SCC is connected to the common crus.

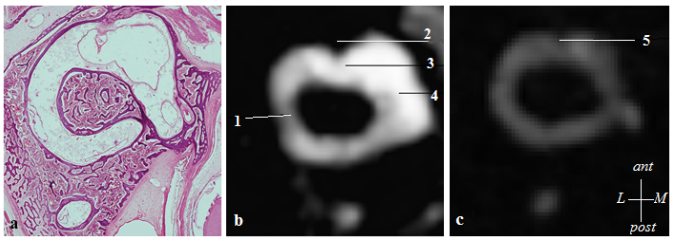

Figure 2. 2a. Histological slice of a human inner ear showing the anterior insertion of the crista in the horizontal duct ampulla (4). Figure 2b: Axial slice of the right semicircular duct in a vestibular schwannoma (3T MRI). The contrast between the endolympathic and perilymphatic spaces is increased. The lateral crista appears in hyposignal. 1: perilymph, 2: lateral crista, 3: lateral ampulla filled with endolymph, 4: utricle. Figure 2c: Axial section of the horizontal SCC duct of a normal inner ear (3T MRI FIESTA sequence). 5: The lateral crista appears in hyposignal (12)

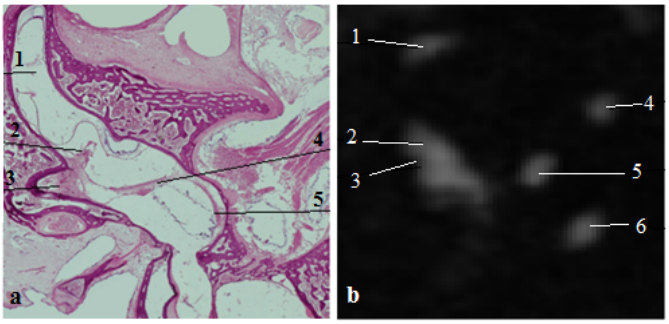

Figure 3 a: Frontal histological slice of the human inner ear. The crista of the anterior semicircular duct is visible at the antero-external part of the ampulla (4). 1: anterior duct, 2: lateral crista, 3: lateral duct, 4: horizontal part of the utricular macula, 5: saccular macula. Figure 3 b: Sagittal slice of the anterior semicircular ampulla (3T Siemens MRI, Fiesta sequence, (10)). 1: anterior duct, 2: anterior ampulla, 3: anterior crista appearing in hyposignal, 4: posterior duct, 5: common crus, 6: posterior duct

Common crus: The common crus present an elliptic section shape. The membranous duct occupies half of the bone duct.

The utricular macula: The utricle has an ovoid shape, lying down in the horizontal plane. The utricular macula is composed of a horizontal part, which is in the same plane as the lateral SCC, and of an anterior vertical partion, which is strongly attached to the bony walls [12]. Thus, the utricular macula presents an L-shaped profile, evoking a "flying carpet". The length of the utricle measures 5 mm, and its height is 1.4 mm. The thickness of the utricular floor is about 0.5 mm.

The saccular macula: The saccular macula is attached to the internal part of the saccule. The normal dimensions of the saccule range from 1 to 1.6 mm in a cranio-caudal plane, and from 1 to 1.4 mm along the transversal direction [12].

3D reconstruction of the posterior membranous labyrinth

Once the final geometry of the surface of the model was obtained, it consisted of 13,939 nodes and 27,873 triangular elements. The volume inside this surface was then filled with a total of 96,828 tetrahedral 3D elements (4,713 elements for the anterior cupula/crista, 3,926 for the lateral cupula/crista, 2,989 for the posterior cupula/crista, 3,195 for the utricular macula, 552 for the saccular macula, and the remaining 81,453 ones for the endolymph). The average edge length for one element is 0.1 mm. Special attention was given to the cupular diaphragms: the borders between cupulas and their surrounding endolymph were designed to be planar; the diaphragms were made of three layers, and the crista was always in the central layer (as seen on Figure 4e). The resulting mesh includes 124,701 elements and 23,977 nodes.

Figure 4a: Anterior view of the model. The positions of the cupulas and cristas of the SCC appear in blue. The position of the utricular macula appears in green. **Figure 4b**: Anterior transparent view of the model, showing the 3D utricular and saccular maculas inside. **Figure 4c:** Anterior view of the model: the parts attached to the bony canal are represented in blue. The mobile parts are represented in red. **Figure 4d:** The 3D utricular macula (the striola is represented). **Figure 4e:** The 3D central layer of the posterior crista and cupula. **Figure 4f:** The posterior ampulla, and the short arm.

Validity study of the geometry of the 3D model of membranous posterior labyrinth

We measured the different parts of the model with the Hypermesh software and compared the values with those in the literature (Figure 5). Results are shown in Table 1.

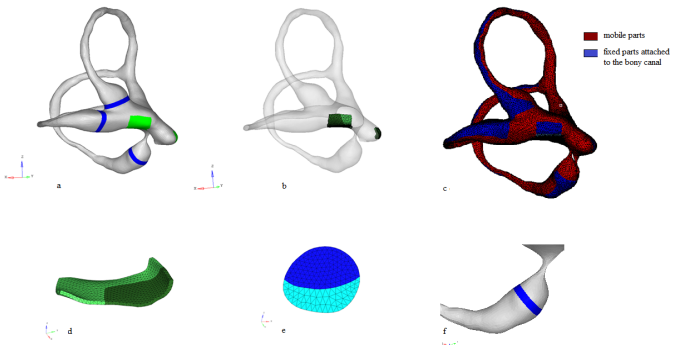

Figure 4 a: Anterior view of the model. The cristas of the SCC appear in blue. The utricular macula appears in green. Figure 4 b: Anterior view of the model, showing the utricular and saccular macula. Figure 4 c: Anterior view of the 3D model: the "fixed" parts are represented in blue. The mobile parts are represented in red. Figure 4 d: 3D utricular macula (the striola is represented). Figure 4 e: Posterior crista and cupula. Figure 4 f: The posterior ampulla, cupula and short arm

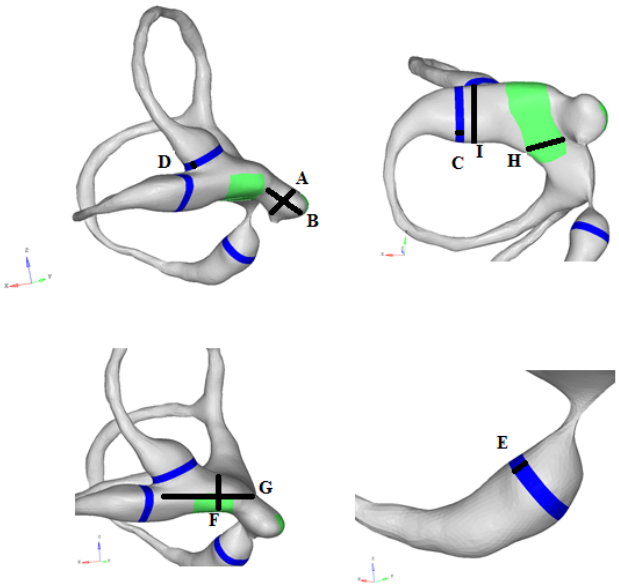

Figure 5. Measured dimensions of the model

Each ampullar crista and cupula is 1.5 mm long and 0.3 mm wide [12]. The average diameter of the lateral semicircular canal ampulla is 2.1 mm. The diameter of the bony lateral canal in the other parts of the canal is about 1.3 to 1.4 mm. The average diameter of the anterior bone canal is 0.8 mm.

These dimensions are close to those mentioned by Veillon [12] and Curthoys [6]. The other dimensions, which were not described in the literature, were measured in a histological atlas of human temporal bone [4]. These are reported in Table 2.

In our model, the angle between the planes of the lateral and anterior semi-circular canals measures about 88°CC, the angle between the anterior and posterior canals measures about 87°CC, and the angle between the lateral and posterior canals measures about 90°CC. Thus, the canals of this model are nearly orthogonal.

Discussion

As this 3D model of the posterior membranous labyrinth was reconstructed based on *in vivo* imaging of a human temporal bone, it has the specificity of being morphologically accurate.

This is made possible by recent advances in imaging of the membranous labyrinth. Contouring of the endolymph is now possible on T2 weighted gradient-echo images in obstructive vestibular schwannoma, due to the increase of perilymphatic protides, which itself increases the contrast between the perilymph and the endolymph. The contours of the utricle, the saccule, the ampulla, and the common crus became identifiable. This differentiation between the endolymph and the perilymph was made possible because of their different protein concentrations and is only possible when using gradient-echo sequences compared to spin-echo sequences, which are not sensitive to protein changes.

To our knowledge, this is the first 3D human posterior membranous labyrinth mesh created from *in vivo* acquired MRI images, and specifying the positions of all of the five sensory zones. Other 3D-modeling works of the human membranous labyrinth already exist, but most of them were developed from *post mortem* studies of temporal bones [1,2,13]. The model of Rajguru et al. [2]

Table 2. Model dimensions against measures from a histological atlas

	Diameters	Measure in the model (mm)	Measure in the histological atlas (4)
J	Average diameter of the posterior ampullar canal	0.3	0.3 to 0.5
K	Diameter of the posterior ampulla at the level of the crista	1.47	1.52
L	Posterior SCC : average diameter of the membranous canal	0.5	0.41 to 0.47
M	Diameter of the anterior ampulla at the level of the crista	1.78	1.57
N	Anterior SCC : average diameter of the membranous canal	0.5	0.38 to 0.53
O	Common crus : main axis	1.33	1.43
P	Common crus : small axis	0.8	0.85

includes the three SCCs, the common crus and the utricle, but the saccule and the positions of sensors were not represented. This model was also used by Shen and al to perform. [13] a numerical simulation of the caloric test. On their model the positions of the anterior, lateral and posterior cupula were specified. The model of Teranishi et al [1] included the entire membranous labyrinth without indicating the sensory areas. In another study by Wu et al, using guinea pig, membranous labyrinth modeling was performed by segmenting micro-CT imaging acquired *post mortem* after impregnating the temporal bone with an osmium tetroxide solution [14]. Several teams have also carried out 3D-modeling of the human bone labyrinth by segmentation of temporal bone CT *in vivo* [20-22].

However, distinguishing the membranous labyrinth from the bony one in the canals remained difficult. Moreover, we faced the limitations of current imaging resolutions of MR devices (although we used a high field 3 Tesla magnet). The size of a voxel (0.3 mm x 0.3 mm x 0.3 mm) approximated the diameter of the membranous canals, so the reconstruction of a canal could only be done from a single row of voxels chosen manually during segmentation. As some canals showed strong curvatures, the first rendering obtained was irregular and rough in certain places. This is why we had to manually rework the SCCs shape using the Hypermesh software. Some elements have been replaced to fill the gaps and create more regular contours. Additional smoothing of the mesh resulted in a final satisfying render.

The study of the positioning of the sensory cristas and maculae has benefited from the unique histological atlas of Sick and Veillon [4]. These histological sections have the advantage of having been carried out in a radiological cutting plane of the lateral canals, which made it possible to carry out a radiological-histological correlation. These histological sections were made from eight fetal temporal bones of at least 7 months. At this age the inner ear is comparable to that of the adult human, since the development of the inner ear reaches adult size around 17 to 19 weeks of gestation [5].

Histological sections may nevertheless contain artefacts which would be related to the preparation. The validity of each histological criterion was studied on their invariance through the axial, sagittal and frontal histological sections. These criteria were also compared with other published histological sections [6-8].

In our study, the validity of the standard geometrical model was achieved by verifying that the dimensions of the different structures, and the orientations of the three canals, were in reasonable agreement with the standards from the literature [6-12].

The canals in the model appear nearly orthogonal. This is coherent with several histological and CT measurements concerning the angular orientation of the bony SCCs. Most conclude that the canal planes are nearly orthogonal [15-18]. Blanks and al [19] ough, report from a study on 10 skulls an average angle, between the lateral canal and the anterior canal planes, measuring 111.8 °CC ± 7.6 °CC. This study did not, however, use a 3D reconstruction process, unlike the others. Della Santina and al [20] analyzed the orientation of the human semicircular bone canals after 3D reconstruction of a larger sample of 44 normal temporal bones, from multi-planar scans of 0.5 mm thickness. The study was in favor of the quasi-orthogonality of the bone canals. They observed an average angle of 90.6 ± 6.2°CC between the anterior and horizontal canals, of 90.4 ± 4.9°CC between the posterior and horizontal canals, and of 94 ± 4°CC between the anterior and posterior canals.

Moreover, the SCCs of our model were not perfectly planar, but instead slightly bent. This non-flatness has been described by Bradshaw and al [21] based on the 3D reconstruction of the bone canals of 34 internal ears.

There are, however, known anatomical variations of the membranous labyrinth. According to Bradshaw and al [21], the angle variation between the anterior and posterior bony canals was respectively ± 3.4°CC, ± 4.4°CC between the anterior and horizontal canals, and ± 5.2°C between the posterior and horizontal canals. In the study by Della Santina and al. [20], the variation in angle between the anterior and posterior bone canals was ± 4°C, ± 6.2°C between the anterior and horizontal canals, and ± 4.9°C between the posterior and horizontal canals. Their study also described a variability in the angle between the lateral canal plane and the Reid reference plane (passing by the orbital level and through the center of the external acoustic meatus): the direction angles between a normal vector to the left horizontal SCC and the positive Reid's stereotaxic X (+nasal), Y (+left), and Z (+superior) axis were 108.7°C +/- 7.5°C, 92.2°C +/- 5.7°C, and 19.9°C +/- 7°C.

As such, the geometry of our model was validated. This morphologically precise model presents several interests: it could be used as a pedagogical tool for the learning of the anatomy of the vestibule. We also experienced that it can be useful in daily clinical practice, serving as a basis for reflection in the contexts of atypical BPPV.

Another perspective of this work is to add material properties to the elements of our model of the posterior membranous labyrinth to create a complete mechanical FEM. Such an approach would be useful to study the biomechanical behaviors of the vestibule, which is one of the major mechanisms of vestibular physiology, and which several vestibular pathologies are linked to (such as hydrops, Meniere's disease, or BPPV). It would also allow the analysis of complex biomechanical phenomena, which are hard to observe and almost impossible to measure *in vivo*, by making numerical estimations. Specific areas may be studied, such as the maculae and the cristas, which are the sensors for movement, with a focus on the stresses and deformations they undergo during movements of the head. Globally, the FEM could be used for the analysis of physiological (spontaneous head movements), pathological (BPPV and positional tests, dynamic exploration of vestibular deficits), or therapeutic situations (study of canal plugging).

Conclusion

In this study, we describe a 3D reconstruction of the posterior membranous labyrinth, using *in vivo* 3T MRI-acquired images of the

temporal bone region with vestibular schwannoma. In this patient, the geometry of the vestibule is preserved but the elevation of perilymphatic protides generates an increase in contrast with the endolymph, which allows its contouring. The 3D external volume was obtained by manual segmentation, with the ITK-Snap software. We then achieved a mesh of the model used for the compartmentalization of the various structures. The position of the anterior crista, lateral crista, posterior crista, utricular macula and saccular macula are represented. This model of a 3D posterior membranous labyrinth has the specificity of being morphologically accurate.

This model is of pedagogical interest for the teaching of anatomy, of vestibular physiology and of positional diagnostic and therapeutic maneuvers. Those interests could be interesting for ENT practitioners as much as vestibular physiotherapists or medical students. This model could also be useful for the clinical reflexion in cases of atypical BPPV. Another perspective is a further use of the 3D model of membranous labyrinth as a mesh upon which a complete mechanical FEM can be built to study the mechanical vestibular physiology.

Acknowledgements

Compliance with ethical standards

Guarantor: The scientific guarantor of this publication is Pr Anne Charpiot.

Conflicts of interest

The authors of this manuscript declare no relationships with any companies, whose products or services may be related to the subject matter of the article.

Funding

This study has received funding: Scholarship from AFON (Association Française d'OtoNeurologie) during the master's degree of Dr Hella VUONG CHANEY.

Statistics and biometry

No complex statistical methods were necessary for this paper.

Informed consent

Written informed consent was obtained from the patient in this study.

Ethical approval

Institutional Review Board approval was not required because the article does not contain patient data.

References

1. Teranishi M, Yoshida T, Katayama N, Hayashi H, Otake H, et al. (2009) 3D computerized model of endolymphatic hydrops from specimens of temporal bone. *Acta Otolaryngol Suppl 3*: 43-47. [Crossref]

2. Rajguru SM, Ifediba MA, Rabbitt RD (2004) Three-dimensional biomechanical model of benign paroxysmal positional vertigo. *Ann Biomed Eng Juin* 32: 831-846.

3. David R, Stoessel A, Berthoz A, Spoor F, et al. (2016) Assessing morphology and function of the semicircular duct system: introducing new in-situ visualization and software toolbox. *Sci Rep 6*: 32772. [Crossref]

4. Sick H, Veillon F (1988) Atlas de coupes sériées de l'os temporal et de sa région. Anatomie et Tomodensitométrie. Spinger-Verlag. New York, Berlin: *J.F Bergmann Verlag Munchen* 161.

5. Jeffery N, Spoor F (2004) Prenatal growth and development of the modern human labyrinth. *J Anat* 204: 71-92. [Crossref]

6. Curthoys IS, Oman CM (1987) Dimensions of the horizontal semicircular duct, ampulla and utricle in the human. *Acta Otolaryngol (Stockh) Juin* 103: 254-261.

7. Schuknecht HF, Gulya AJ (1986) Anatomy of the Temporal Bone with Surgical Implications. Philadelphia: Lea and Febiger: 350.

8. Schuknecht HF (1993) Pathology of the Ear. 2ème édition. Malvern, Pennsylvania: Lea and Febiger; 1993. 672.

9. Venkatasmy A, Le Foll D, Karol A et al. (2017) Differentiation of vestibular schwannoma from meningiomas of the internal auditory canal using perilymphatic signal evaluation on T2-weighted gradient echo fast imaging employing steady stade acquisition at 3T. European Radiology Experimental 2017. Mai 2017, 1: 8.

10. Yushkevich PA, Piven J, Hazlett HC, Smith RG, Ho S, et al. (2006) User-guided 3D active contour segmentation of anatomical structures: significantly improved efficiency and reliability. *Neuroimage* 31: 1116-1128. [Crossref]

11. Cignoni P, Callieri M, Corsini M, Dellepiane M, Ganovelli F, Ranzuglia G, et al. (2008) MeshLab: an Open-Source Mesh Processing Tool Sixth Eurographics. *Italian Chapter Conference* 13: 129-136.

12. Veillon F (2008) Imagerie de l'oreille et de l'os temporal, anatomie et imagerie normales. *Lavoisier Médecine Sciences Publications* 1: 339

13. Shen S, Liu Y, Sun X, Zhao W, Su Y, et al. (2013) A biomechanical model of the inner ear: numerical simulation of the caloric test. *Scientific World Journal* 160205. [Crossref]

14. Wu C, Wang K (2011) Three-dimensional models of the membranous vestibular labyrinth in the guinea pig inner ear. 4th International Conference of Biomedical Engineering and Informatics.

15. Wang T, An F, Xie C, Chen J, Zhu C, Wang Y, et al. (2014) The treatment of benign positional paroxysmal vertigo of posterior semicircular canal by Epley maneuver combined with Semont maneuver. Lin Chuang Er Bi Yan Hou Tou Jing Wai Ke Za Zhi. *J Clin Otorhinolaryngol Head Neck Surg* 28: 1469-1471.

16. Archer CR, Cooper MH, Kveton JF (1988) Correlation of high-resolution computed tomography and gross anatomic sections of the temporal bone: II. Vestibular apparatus. *Am J Otol Juill* 9: 276-281.

17. Takagi A, Sando I, Takahashi H (1989) Computer-aided three-dimensional reconstruction and measurement of semicircular canals and their cristae in man. *Acta Otolaryngol (Stockh). Juin* 107: 362-365.

18. Spoor F, Zonneveld F (1998) Comparative review of the human bony labyrinth. Am J Phys Anthropol Suppl 27: 211-251. [Crossref]

19. Blanks RH, Curthoys IS, Markham CH (1975) Planar relationships of the semicircular canals in man. *Acta Otolaryngol* 80: 185-196. [Crossref]

20. Della Santina CC, Potyagaylo V, Migliaccio AA, Minor LB, Carey JP, et al. (2005) Orientation of Human Semicircular Canals Measured by Three-Dimensional Multiplanar CT Reconstruction. *JARO J Assoc Res Otolaryngol* 6: 191-206.

21. Bradshaw AP, Curthoys IS, Todd MJ (2010) A mathematical model of human semicircular canal geometry: a new basis for interpreting vestibular physiology. *J Assoc Res Otolaryngol JARO Juin* 11: 145-159.

22. Lee J-Y, Shin K-J, Kim J-N, Yoo J-Y, Song W-C, Koh K-S, et al. (2007) A morphometric study of the semicircular canals using micro-CT images in three-dimensional reconstruction. *Anat Rec Hoboken NJ Mai* 296: 834-839.